Multiple-gradient array measurements for multichannel 2D resistivity imaging

Dahlin, Torleif; Zhou, Bing

Published in:
Near Surface Geophysics

2006

Near Surface Geophysics, 2006, 113-123

Multiple-gradient array measurements for multichannel 2D resistivity imaging

Torleif Dahlin[1*] and Bing Zhou[2]

[1] *Engineering Geology, Lund University, Box 118, S-221 00 Lund, Sweden*
[2] *Dept. of Physics, The University of Adelaide, SA 5005, Australia*

Received November 2003, revision accepted September 2005

ABSTRACT

Two-dimensional resistivity imaging using multiple gradient, Wenner and dipole-dipole electrode arrays was carried out at two field sites in Sweden and one in Nicaragua, with the objective of confirming the practical applicability of results obtained with numerical modelling. The results support earlier numerical modelling studies that concluded that the gradient array, using multiple current electrode combinations, has resolution as good as or better than the commonly used Wenner array. The array behaved well in terms of sensitivity to noise at the test sites, and the results obtained generally agree with dipole-dipole array results, although the latter at two of the sites gave resistivities that differed significantly from the other arrays in the deeper parts of the inverted models. A formula proposed for pseudosection plotting works well for data quality assessment, where it can be an advantage to make separate plots for each *m*-factor (the distance between the midpoints of the current and potential electrode pairs) or for each *a*-spacing. The gradient array is well suited for multichannel data acquisition, and can significantly increase the speed of data acquisition in the field and at the same time give higher data density, but it is also an attractive option for single-channel data acquisition. The Wenner array, on the other hand, is not suitable for measuring in more than one channel. Compared to the dipole-dipole array, it offers lower sensitivity to noise which may be a major advantage in real data acquisition, and the remote electrode needed for the pole-dipole array is avoided, which is often a significant advantage for field logistics.

INTRODUCTION

Resistivity imaging is becoming increasingly popular in electrical exploration, due to its ability to produce images of the subsurface efficiently and effectively as a result of the availability of automated data-acquisition systems and efficient user-friendly inversion software. One of the major limitations of the technique today is the time-consuming measurement process that tempts data-acquisition teams to reduce the data density in order to save expensive field operation time, which in turn can be devastating for the imaging quality. In a previous paper (Dahlin and Zhou 2004), two electrode configurations suitable for multichannel recording, i.e. the multiple gradient array and the midpoint-potential-referred measurement, were presented. These electrode configurations are well suited for multichannel data-acquisition systems, so that many data points can be recorded simultaneously for each current injection, thus reducing fieldwork time significantly without compromising the data density. These two arrays were numerically examined for 2D resistivity imaging, along with conventionally used electrode arrays, such as the Wenner-α, Schlumberger, dipole-dipole, pole-dipole and pole-pole arrays. The work concluded that the gradient array gives the best imaging resolution of the two, and it is as good as the best of the conventionally used arrays, which were found to be Schlumberger, dipole-dipole and pole-dipole. This paper can thus be regarded as part 2 of our previous paper, and for numerical modelling results the reader is referred to Dahlin and Zhou (2004).

The aim here is to test the practical applicability of multiple-gradient-array surveying, and to compare its performance with traditionally used electrode arrays. Results from field tests carried out at the three following sites are presented: (1) a waste dump, (2) a shallow layered sequence with a faulted zone and (3) an esker resting on the edge of a horst. For practical reasons, the comparisons with traditional arrays are restricted to the Wenner and dipole-dipole arrays. Although our numerical modelling (Dahlin and Zhou 2004) shows that pole-dipole is a strong candidate, it was not included in the tests presented here as it is often not practical in routine application, which is the focus of this work, due to the need for a remote electrode.

* Torleif.Dahlin@tg.lth.se

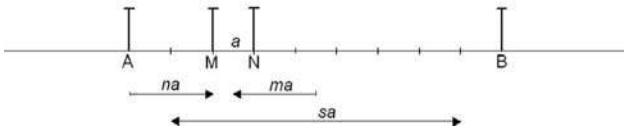

FIGURE 1
Sketch of gradient array showing the position of the electrodes for a measurement with a current-electrode separation of $(s+2)a$, where the separation factor $s = 7$, the n-factor = 2 and the midpoint factor $m = -2$. Here, the n-factor is defined as the smallest relative spacing between a current electrode and a potential electrode.

MULTI-ELECTRODE GRADIENT SURVEYING

Multi-electrode gradient surveying is carried out by injecting current with a separation $(s+2)a$ (see Fig. 1) and simultaneously or sequentially picking up all the potential differences between the potential electrodes with spacing a. Here, the separation factor s, an integer, is the maximum number of potential readings for a current injection. The factor n can here be defined as the relative spacing between the potential dipole and the closest current electrode. Furthermore, it can be practical to define a midpoint factor m as the position of the midpoint of the potential electrode dipole relative to the midpoint of the two current electrodes, i.e.

$$m = \frac{(x_M + x_N)/2 - (x_A + x_B)/2}{(x_N - x_M)} = \frac{x_{MN} - x_{AB}}{a}, \qquad (1)$$

where x_A, x_B, x_M, x_N are the positions of the current and potential electrodes ($x_B > x_A$, $x_N > x_M$), and x_{AB}, x_{MN} are the midpoints of the respective dipoles. Hence, a negative m-factor indicates a potential dipole to the left of the current electrode midpoint, and a positive m-factor indicates that the potential electrode dipole is shifted to the right, relative to the midpoint. Similarly, for data handling purposes, it may be convenient to define the n-factor as a vector, with positive n-factors when the potential electrodes are at higher coordinates than the closest current electrode and negative n-factors when they are at lower coordinates. It follows that, for given s and n values, m is also determined as

$$m = n - \frac{s+1}{2}, \qquad \text{for } x_{MN} \le x_{AB} \ (m \le 0), \qquad (2)$$

and

$$m = n + \frac{s+1}{2}, \qquad \text{for } x_{MN} > x_{AB} \ (m > 0), \qquad (3)$$

where n and m are negative or positive integers.

Figure 2(a–c) shows examples of three positions of the potential electrodes for the gradient array, with the corresponding sensitivity function (McGillivray and Oldenburg 1990; Loke and Barker 1995) on homogeneous ground. Generally, the larger the relative separation of current and potential electrodes, the deeper is the penetration of the configuration. In practical applications, the selection of the spacing a and the separation s will depend on a trade-off between noise sensitivity, horizontal detail and depth

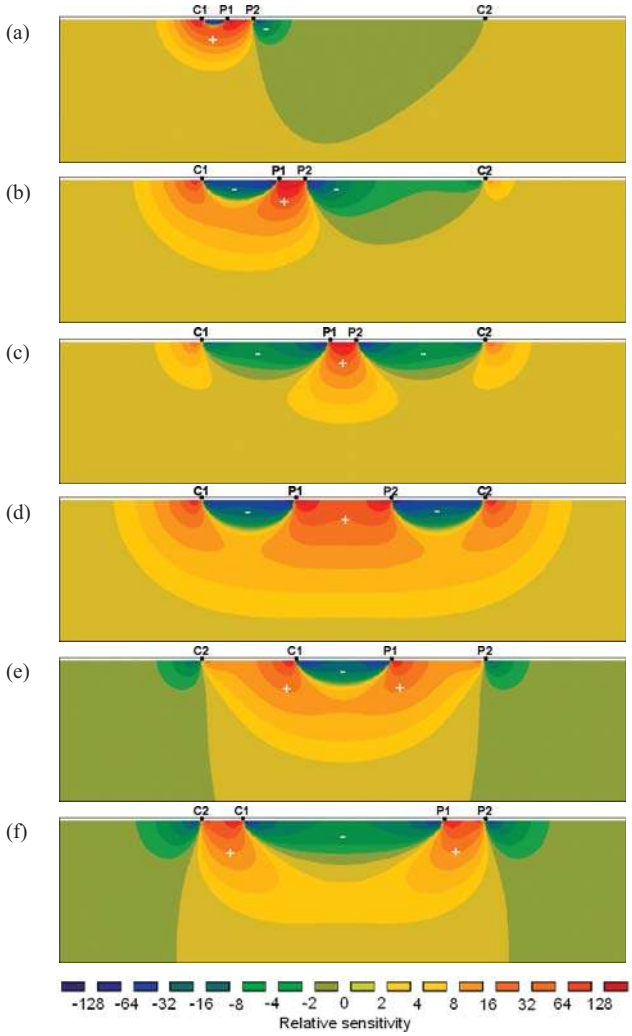

FIGURE 2
Vertical section through a 3D sensitivity function along the electrode layout for example electrode arrays: (a) gradient ($s = 9$, $n = 1$); (b) gradient ($s = 9$, $n = 3$); (c) gradient ($s = 9$, $n = 5$); (d) Wenner; (e) dipole-dipole ($n = 1$); (f) dipole-dipole ($n = 5$). C1 and C2 denote current electrodes; P1 and P2 denote potential electrodes. Regions marked with (+) have positive sensitivity and those with (–) have negative sensitivity. Vertical-horizontal plot ratio = 1. The absolute scale is the same for all diagrams, exept for (a) (damped one magnitued) and (f) (amplified one magnitude).

penetration. Traditional gradient surveying often comprised measurements with the current electrodes at one fixed location only. In a multi-electrode gradient survey, a large number of current electrode combinations are used, scanning across the electrode layout with several different spacings a and/or separations s, similar to multi-electrode surveying with other electrode arrays.

It can be observed that the gradient array is essentially a pole-dipole array when the potential dipole is close to one of the current electrodes (Fig. 2a), at least for large s-factors. When the potential dipole is centred between the current electrodes, it is equal to the Schlumberger array (Fig. 2c). Thus, the gradient

array may be expected to combine the characteristics of the pole-dipole, Wenner and Schlumberger arrays; however, without the need for a remote electrode, this can be cumbersome to arrange in some environments.

For comparison, sensitivity functions for the Wenner and dipole-dipole arrays are also shown (Fig. 2d,e). For the Wenner array (Fig. 2d), it is evident that the lateral sensitivity is less focused, which suggests poorer definition of narrow vertical features, whereas the sensitivity has a slightly more rapid roll-off with depth, which is good for defining the depth to layer interfaces. The sensitivity pattern of the dipole-dipole array depends on the *n*-factor (Fig. 2e,f), as shown by the two examples. For *n*-factors larger than one, it has a distinct vertical character, indicating good resolution capability for vertical structures, whereas it rolls-off very gradually with depth, which suggests relatively poor definition of depth to horizontal boundaries. It is also noteworthy that the dipole-dipole array has a high sensitivity near the ends of the layout, but little sensitivity at the centre where the data are normally plotted in a pseudosection.

The median depth of investigation (Edwards 1997) for a certain current electrode separation varies, depending on the relative position of the potential dipole, as illustrated by examples in Table 1 (s = 9 and 18), hence fewer different current-electrode separations are needed for a good depth cover in an imaging survey with a multiple-gradient array than with, for example, a Wenner array. The signal-to-noise ratio also varies with the relative position of the potential electrodes, being highest close to a current electrode and lowest at the centre of the layout. Table 1 also shows the relative signal-to-noise ratio. This is based on normalizing the inverse of the geometry factor against that of the Wenner array, which has the highest signal-to-noise ratio of the commonly used arrays, in order to make it independent of the size of the layout. The dipole-dipole array has a slightly larger depth penetration for the larger *n*-factors, but *n*-factors over 2 already give signal-to-noise ratios below the lowest of the gradient array with an *s*-factor of 18, and, for example, for an *n*-factor of 8 it is more than a magnitude lower than the lowest of the gradient-array examples in Table 1. Since the noise in field data is closely related to the magnitude of the measured potentials (Zhou and Dahlin 2003), this can be a very important consideration in survey planning.

TABLE 1

Median depth of investigation, geometry factor and relative signal-to-noise ratio (S/N-ratio relative to Wenner array) for the Wenner, dipole-dipole and gradient arrays (examples for two different s-factors). The total electrode layout length is 1 in all cases. Note that the gradient array configuration with s-factor 9 and n-factor 5 is identical to the Schlumberger array with n-factor 4

Array	***a***	***s***	***n***	**Median depth**	**Geometry factor**	**Relative S/N-ratio**
Wenner	0,3333	-	-	0,1730	2,09	1
Gradient	0,0909	9	1	0,0481	1,12	1,874
Gradient	0,0909	9	2	0,0897	3,16	0,662
Gradient	0,0909	9	3	0,1347	5,64	0,371
Gradient	0,0909	9	4	0,1743	7,74	0,271
Gradient	0,0909	9	5	0,1902	8,57	0,244
Gradient	0,05	18	1	0,0261	0,62	3,353
Gradient	0,05	18	2	0,0471	1,85	1,133
Gradient	0,05	18	3	0,0683	3,61	0,580
Gradient	0,05	18	4	0,0909	5,80	0,361
Gradient	0,05	18	5	0,1150	8,25	0,254
Gradient	0,05	18	6	0,1397	10,72	0,195
Gradient	0,05	18	7	0,1626	12,95	0,162
Gradient	0,05	18	8	0,1804	14,64	0,143
Gradient	0,05	18	9	0,1900	15,55	0,135
Dipole-dipole	0,3333		1	0,1386	6,28	0,333
Dipole-dipole	0,25		2	0,1743	18,85	0,111
Dipole-dipole	0,2		3	0,1923	37,70	0,056
Dipole-dipole	0,1667		4	0,2034	62,83	0,033
Dipole-dipole	0,1429		5	0,2108	94,18	0,022
Dipole-dipole	0,125		6	0,2162	131,95	0,016
Dipole-dipole	0,1111		7	0,2204	175,97	0,012
Dipole-dipole	0,1		8	0,2236	226,19	0,009

PSEUDOSECTION PLOTTING

Plotting the measured apparent resistivities as a pseudosection is a valuable tool for fast assessment of the data quality. Such fast and easy-to-use tools are important in order to make it feasible to check data quality in the field, so that potential data-quality problems can be discovered and addressed as early as possible. Consistent, although not necessarily very smooth, variation of apparent resistivity in a pseudosection shows that the data quality is acceptable. A modestly experienced field crew easily picks out data outliers indicating measurement or technical problems for a symmetrical array like the Wenner. A pseudosection can also give a rough indication of the resistivity structure at the site, but it must be used with great caution as the different sensitivity functions of each of the electrode arrays may lead to pseudosection images that are strongly distorted compared to the geometry of the imaged structures. Pseudosection plotting is also valuable as a step in checking the data quality before inverting the data, along with data editing using other tools.

Pseudosection plotting for commonly used electrode arrays, such as the Wenner, is straightforward (Edwards 1977). In order to plot an apparent-resistivity pseudosection for the gradient configuration, the following formulae for calculating the plot position (x_{ρ_a}, z_{ρ_a}) of an apparent resistivity ρ_a are proposed:

$$x_{\rho_a} = x_{MN}, \tag{4}$$

$$z_{\rho_a} = \min\{(x_{MN} - x_A), (x_B - x_{MN})\}/3, \tag{5}$$

where x_{MN} is the midpoint of the potential electrode pair *M*, *N*, and x_A and x_B are the current electrode positions *A*, *B* (see Fig. 3). The depth-reduction factor 3 was chosen arbitrarily for z_{ρ_a} to be roughly in the same range as the median depth of investigation.

For the gradient protocols we have tested, many data points end up in the same location in the pseudosection, notably the data points measured with the same potential-electrode positions but mirrored current-electrode positions. As these data points are not sensing the same volume of earth, they will differ in measured value except in homogeneous or horizontally layered earth. Hence, it is suggested that pseudosections based on several subsets of the data are plotted separately for data-quality assessment purposes.

An alternative approach, which may be argued as being more physically correct, would be to integrate the sensitivity function (Fig. 2) horizontally for the median depth penetration and vertically to find the point with 50% of the sensitivity on each side. However, as will be demonstrated below, the simple formulae above work well in practice for data-quality assessment purposes.

DATA ACQUISITION AND PROCESSING

The data acquisition at all test sites was performed using different versions of the ABEM Lund Imaging System (Dahlin 1996), including, in some cases, prototype equipment.

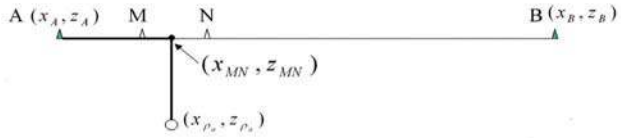

FIGURE 3
Definitions for calculation of pseudosection plot point for gradient array.

All field data were inverted using Res2dinv (versions 3.47i, 3.50a and 3.54r). Although both L_1-norm (robust) and L_2-norm (least-squares) inversions were tried (Loke *et al.* 2003), the results presented here are from the former only, as these results produced images that appeared to be in better accordance with the geology and were more consistent between the electrode arrays. Results from previous work also suggest that L_1-norm inversion often gives more stable results (Zhou and Dahlin 2003; Dahlin and Zhou 2004). The model residual values presented for the inversions are root-mean-square values. The data were inverted using mostly default inversion parameters, using the Gauss–Newton method for recalculating the sensitivity matrix for all iterations in all cases. The data were saved in a general electrode format without information on the electrode array used, in order to avoid possible bias from array-specific inversion parameters of the inversion software. Tests were made inverting the data with a model grid size equal to the smallest electrode spacing in the surveys, and with one equal to half the actual electrode spacing.

FIELD EXAMPLE 1: HÄRLÖV WASTE DEPOSIT

A field test was carried out at the Härlöv waste deposit site in southern Sweden. The waste at the site is mainly of domestic origin, and is covered by soil that varies in thickness and composition, but there are also zones that are dominated by excavation material and/or building demolition waste. The investigation was carried out with the purpose of mapping the soil cover (Leroux and Dahlin 2002). A line measured with three different electrode arrays, Wenner, dipole-dipole and multiple-gradient, is presented here. An electrode spacing of 1 m was used for high resolution of the shallow soil cover. Measurements were, in this case, made with one channel for the Wenner array, and three channels for the other arrays, allowing much more efficient data acquisition for the latter. For the Wenner array, values a = 1, 2, 3, 4, 6, 8, …, 24 m were used. Dipole-dipole measurements were taken using a = 1, 2, 3, 4, 6, 8 m and n = 1, 3, 5, while the multiple-gradient array data were recorded with a = 1, 2, 4, 6 m and s = 9. Favourable electrode grounding conditions allowed transmission of 50–100 mA, which in combination with the short electrode separations gave very stable data. The measurement time, excluding time to set up and move electrodes and cables, was around three hours for the more than 3300 data points of the gradient-array data set. Gradient and dipole-dipole (2223 data points) were equally efficient in terms of speed of data acquisition, whereas the Wenner data recording was slower due to sin-

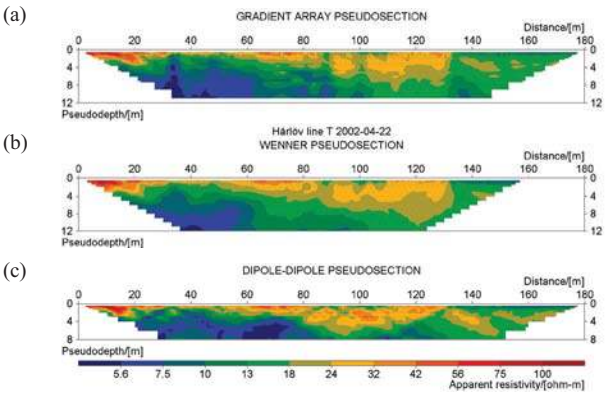

FIGURE 4

Pseudosections based on data measured along Line T at the Härlöv waste deposit site: (a) gradient (a = 1, 2, 3, 4 m); (b) Wenner; (c) dipole-dipole (a = 1, 2, 3, 4, 6, 8 m and n = 1, 3 and 5).

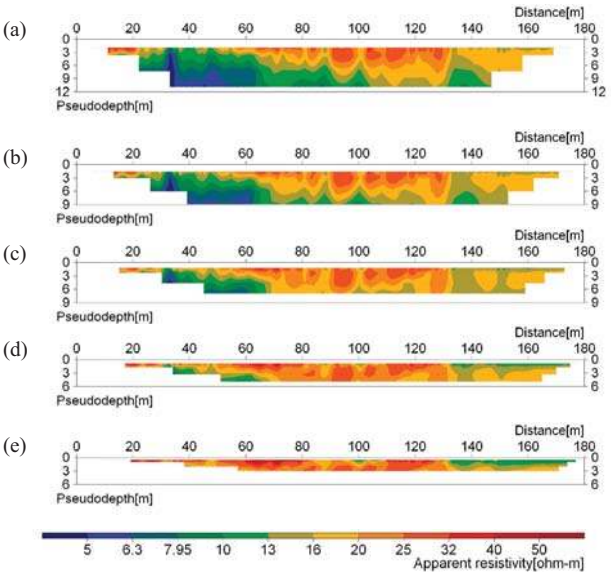

FIGURE 5

Pseudosections based on gradient array data measured along Line T at the Härlöv waste deposit site: (a) m = 0, (b) m = 1, (c) m = 2, (d) m = 3, (e) m = 4. Note that the data plot is incomplete since data for m-factors –4 to –1 are not shown.

gle-channel measuring (1097 data points, if it had the same length as the other arrays it would have been 1260).

Pseudosections from Härlöv are shown in Fig. 4, where the Wenner array result (Fig. 4b) appears to be of good quality. The gradient array and dipole-dipole results (Fig. 4a,c) may give the wrong impression that they are noisier when all the data are plotted together, which is not the case. If the data are plotted for one m-factor (or n-factor) at a time, as demonstrated for the

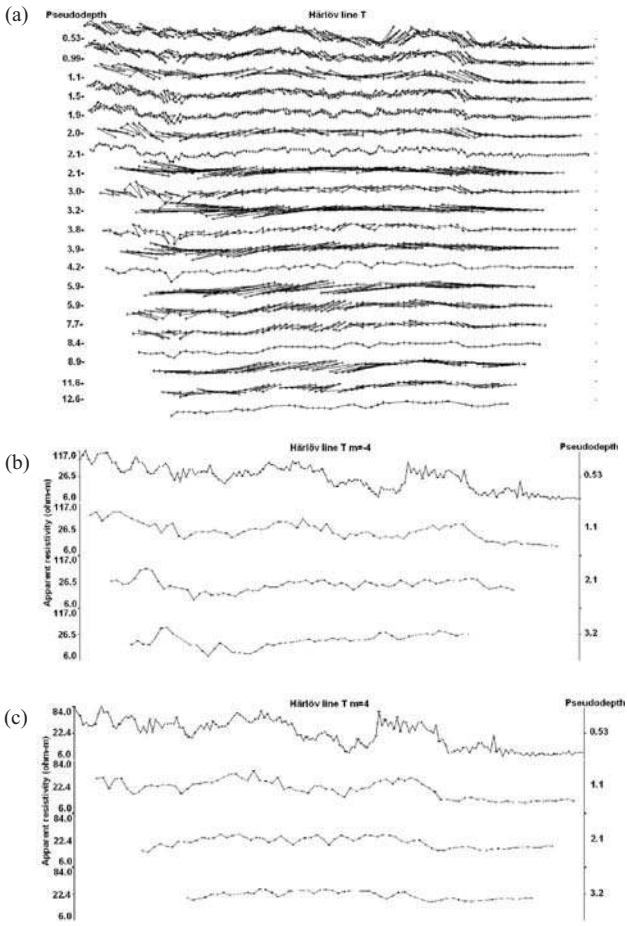

FIGURE 6

Examples of apparent-resistivity plots of gradient- array data measured along Line T at the Härlöv waste deposit site: (a) all data (m = –4, –3, …, 4); (b) m = –4; (c) m = 4.

gradient data (Fig. 5d–g), each pseudosection displays a much more consistent appearance.

For data-quality control and editing purposes, it is often convenient to display the data as a number of profiles with the same median depth of investigation, but doing so with multiple-gradient array data often results in apparently very noisy data (Fig. 6a). This is caused by the mixing of data with positive and negative m-factors (or negative and positive n-factors), and if plotted separately, the same data look consistent, as shown by the examples in Fig. 6(b,c).

Inverted sections from the data are shown in Fig 7. The main character of the inverted sections is similar for all three arrays, exhibiting strongly variable resistivity in the waste. In the deeper parts, significant differences are evident. It can be seen that a narrow vertical zone at 70 m is indicated by all three arrays. However, at 105–110 m, the structure at the bottom of the section is mapped as high resistivity by the Wenner and gradient arrays but as low resistivity by the dipole-dipole array. This may be

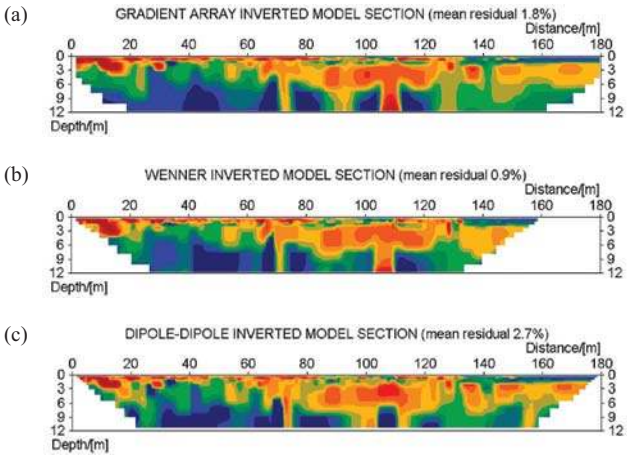

FIGURE 7
Inverted sections for Line T at the Härlöv waste deposit site, based on (a) gradient array, (b) Wenner and (c) dipole-dipole data.

interpreted as being caused by deviations from the 2D assumption that affects the arrays differently, depending on the different sensitivity patterns of the arrays; the lateral 3D variation in resistivity is very strong at the site. Numerical modelling results presented by Dahlin and Loke (1997) suggest that the dipole-dipole array is more sensitive to 3D effects than the Wenner, and although the gradient array was not included in that study it may be expected that it is closer to the Wenner than the dipole-dipole in this respect, due to its sensitivity pattern. The data quality is good for all the electrode arrays tested, although the model residuals are slightly higher for the dipole-dipole array.

According to shallow auger sampling, there is 0.9 m fill consisting of mixed soil at 32 m along the line, underlain by waste. At 82 m, augering went through 2 m of mixed soil without reaching the waste; unfortunately the composition and stratification of the soil and waste was not well documented. Around this point the two shallowest layers visible in the resistivity models can be interpreted as protective soil cover over a clay layer, the latter being intended as an impervious seal to prevent ingress of rainwater. In all three inverted sections, these two top layers can be discerned along parts of the line but they do not appear to be continuous. A similar pattern is manifested along the other lines measured at the site (around 4.5 km in total). The variation in depth to the waste found by augering at more than 30 points in the vicinity confirms the result, with the upper fill material consisting of sand, clay, clayey till, bricks, lime, etc. The variation in resistivity below the top cover depends to some extent on variation in waste composition, but previous studies show that it is difficult to find a correlation between resistivity and waste type, due primarily to variations in water content (Bernstone *et al.* 2000). Auger results and visual inspection of some excavated trenches suggest that this is also the case here. The base of the waste has not been identified in the resistivity results; possibly the result of the small depth of survey investigation or low resistivity contrast with underlying soils.

FIELD EXAMPLE 2: FAULTED VOLCANIC SEDIMENTS IN MANAGUA

The second study site is located within the Rubén Darío Campus of UNAN-Managua, Nicaragua. It is close to a fence and a major road that limits the extension of the test profile at the lower end of the line. The materials underlying Managua City comprise volcanic sediments within the Las Sierras Group, formed between the Late Tertiary and the Quaternary. Above this group, sequences of pyroclastic materials, which constitute the Las Nubes Group and the Managua Group, can be observed. The presence of layers of fossil soils suggests the existence of periods of inactivity between volcanic or tectonic events that allowed the development of the various soil types (Hradecky *et al.* 1997; W. Martínez 2001, *Estudio Geológico de Riesgo Sísmico en Terreno donde se Proyecta Construir los Laboratorios del CIGEO/UNAN, Managua*, unpublished report, Managua). A trench of 2–3 m depth was dug and documented geologically prior to nearby construction works (Fig. 8). The soils are volca-

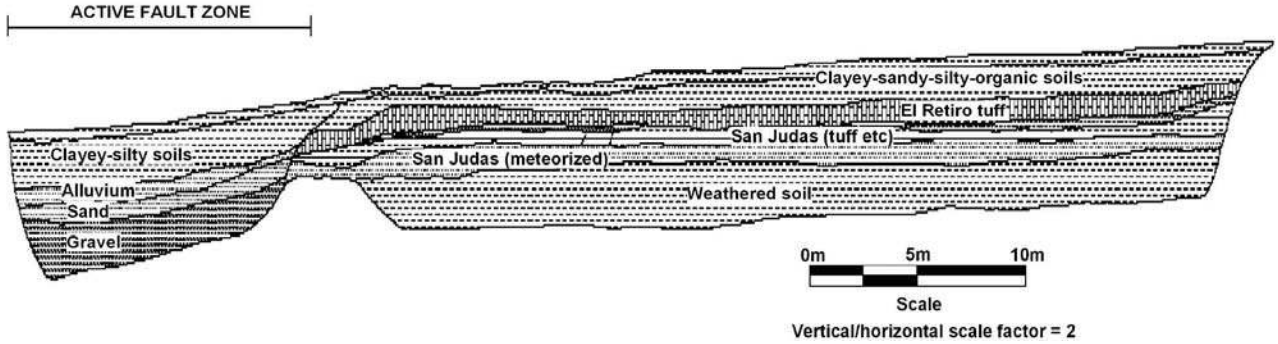

FIGURE 8
Simplified geological section based on documentation from trench at the CIGEO test site in Managua (modified from Martínez 2001, see text). Note that the trench covers only part of the resistivity line.

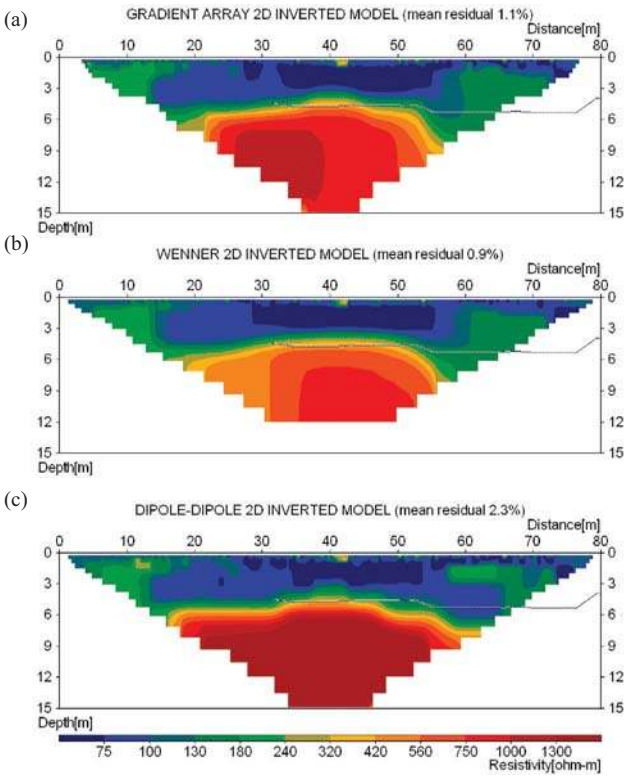

FIGURE 9

Inverted sections from the Managua test line, based on (a) gradient array, (b) Wenner and (c) dipole-dipole data.

no-sedimentary from the Holocene and comprise modern soils, fossil soils, tuff, basaltic sands of black colour and fines, some associated with the San Judas Formation. The soils exhibit a consistent layering throughout the trench section, except in the leftmost part (up to around distance 15–18m) of the trench where a fault zone interrupts the layers (Fig. 8).

The test line was measured parallel to the location of the trench, but offset from it by approximately 5 m for logistical reasons. The slight lateral shift is not expected to cause any dramatic change in the stratigraphy, as verified by shallow auger drilling at selected points along the test line. Unfortunately, the augering did not reach much deeper than the trench, due to the firm formations encountered and the limitations of the augering equipment, so the exact position and characteristics of the bottom layer identified in the resistivity sections presented below could not be checked.

Three different electrode arrays were used: Wenner, dipole-dipole and gradient. For the Wenner data, values $a = 1, 2, 3, 4, 6, \ldots, 24$ m were employed. The dipole-dipole data were measured using $a = 1, 2, 4, 6, 8, 10, 12$ m and $n = 1, 2, 3, 4$, while the gradient-array data were measured using $a = 1, 2, 4, 6, 8$ m and $s = 8$. Good grounding conditions allowed a minimum of 50 mA current to be transmitted, which in combination with the short electrode separations gave stable data. In general, only the longest n-factors for the dipole-dipole array required more than two stacks (maximum variation coefficient 1%). The data sets contain 445, 889 and 1080 data points respectively, and pure measurement time was around 1.5 hours for the gradient array. Since the Wenner data were measured using one instead of four measurement channels as for the other data sets, the actual measurement time was correspondingly longer, compared to each of the larger data sets. The smaller number of data for the dipole-dipole array did not make it faster than the gradient-array data set, since more stacking was made due to weaker signals. Moreover, full advantage of the multichannel measuring capability cannot be taken towards the ends of the layout when measuring with the dipole-dipole array, since one or more channels would be 'outside' the electrode layout when measuring at some of the data points.

The measured pseudosections (not shown) of the different electrode arrays are quite consistent, due to the relatively small lateral variation. The total dynamic is highest in the dipole-dipole data, in terms of minimum and maximum measured apparent resistivities, and it lowest for the Wenner data.

The inverted sections show similar main features (Fig. 9), with low-to-intermediate resistivities in the upper part (down to 5–6 m depth) and high resistivities at the bottom of the section. The faulted zone mapped in the trench (Fig. 8) is clearly visible in the leftmost part of the sections (up to distance 15–20 m). In the upper part, the differences between the electrode arrays are only in small-scale details. The shallow (~1–3 m depth) zone that appears from around distance 57 m and upward might be of similar character but it is just outside the area mapped in the trench.

The dipole-dipole array section exhibits a significantly higher bottom-layer resistivity than the other arrays. Inversion of gradient-array data from an extension of the survey line (Fig. 10) shows a bottom-layer resistivity in accordance with the Wenner and gradient-array sections in Fig. 9. The shallower details of the models agree slightly better with the extended section for the dipole-dipole array than for the other arrays, probably due to the higher sensitivity near the ends of the electrode layout (see Fig. 2).

Seismic refraction results presented by Parrales *et al*. (2003) show a two-layer sequence, with P-wave velocities (V_P) of the

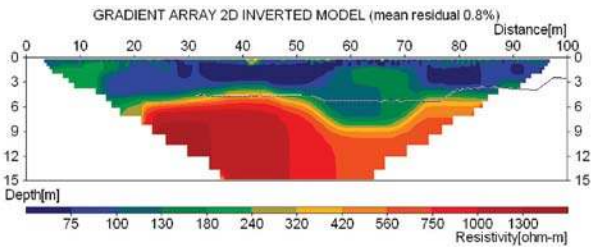

FIGURE 10

Inverted gradient array section of extended line from the CIGEO test site in Managua, with depth to refractor from seismic survey superimposed (Parrales et al. 2003).

first layer averaging 377 m/s, whereas the second layer (refractor) has an average V_P of 590 m/s at depths between 2.5 and 5.3 m. The depth to the bottom layer varies in a manner similar to the seismic refraction survey; however, the dip at 55–75 m is shallower in the seismic refraction result. The refractor and the high-resistivity bottom layer appear to show the same geological features, since the depth to the refractor follows the shape of the depth to the high-resistivity bottom layer (Fig. 10). The discrepancy in depth may be caused by overestimation of the layer thicknesses in the overlying sediments by the resistivity method due to equivalence or anisotropy, or by an existing additional layer with low resistivity but high velocity at 55–75 m.

FIELD EXAMPLE 3: KNIVSÅSEN ESKER

Another field test was carried out over the Knivsåsen esker in southern Sweden. The site is situated close to the northern edge of the Romele Horst, i.e. in connection with a major fault zone where a series of faults can be expected. The part of the area south of the esker is characterized by 0–20 m of till overlying aplitic gneiss, smaller areas of leptitic gneiss and dolerite intrusions. The topography largely follows the bedrock topography. The area north of the investigated line is characterized by clayey sandy till under thin horizons of sand and/or clay. It is assumed that the till in this part of the area is underlain by sedimentary rock (Ekström 1961; Ringberg 1980).

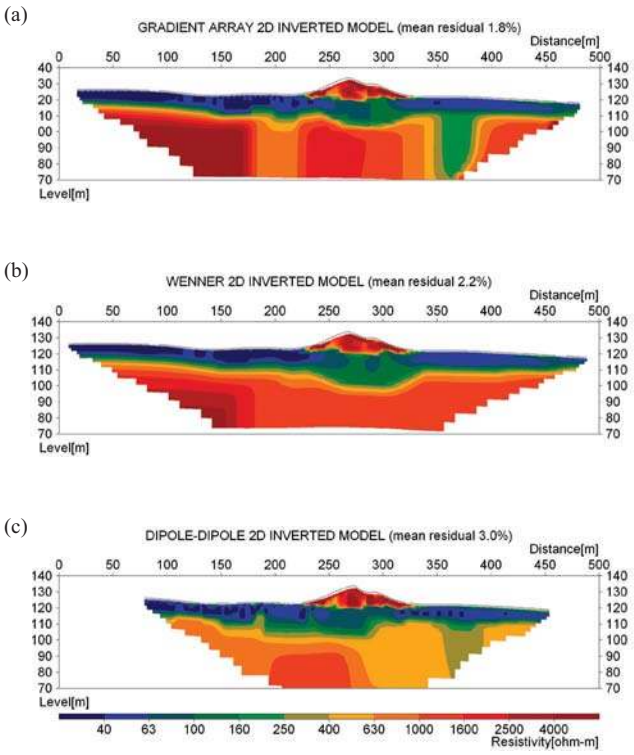

FIGURE 11

Inverted sections across the Knivsåsen esker, based on (a) gradient array, (b) Wenner, (c) dipole-dipole data.

A line measured with the three different electrode arrays is presented here. An electrode spacing of 5 m was used, giving a total electrode cable layout of 400 m. The Wenner survey used a = 5,10,15,12,30, …,120 m, the dipole-dipole survey used a = 5,10,30,50 m and n = 1–6, while the gradient array used a = 5,10,20,30 m and s = 7. Electrode grounding was favourable along most of the line, allowing 100 mA to be transmitted, but problematic across the esker where, despite watering of the electrodes and other efforts, only 5–10 mA could be achieved. The Wenner survey measurements were taken using one channel, whereas multichannel measuring was used for the other arrays. Even if the latter two were measured with a much higher data density, the actual measurements were much faster. The gradient-array data set has a data density more than twice as high as the Wenner array, i.e. 1337 data points compared to 492 data points. Not counting the time required for laying out the electrodes and moving the electrode cables, etc., the gradient array required 1.5 hours for pure measuring whereas the Wenner data took more than 3.5 hours, i.e. the former took less than half the time to measure. In both cases, measuring included registration of time-domain induced polarization that is not presented here, and data were stacked at least twice.

The L_1-norm inverted section based on the gradient data is shown in Fig. 11(a). The upper part of the esker is characterized by high resistivity (>1000 Ωm) that is mainly caused by the dry coarse-glacial-gravel core of the esker, but on the edges there may be washed sandy sediments. At depths corresponding to the ground levels next to the esker, the resistivity drops dramatically (~100 Ωm); according to available information, this coincides with the water table. On each side of the esker, a low-resistivity upper layer is evident, corresponding to clayey till and possibly sedimentary clay (<63 Ωm). These layers rest on high-resistivity

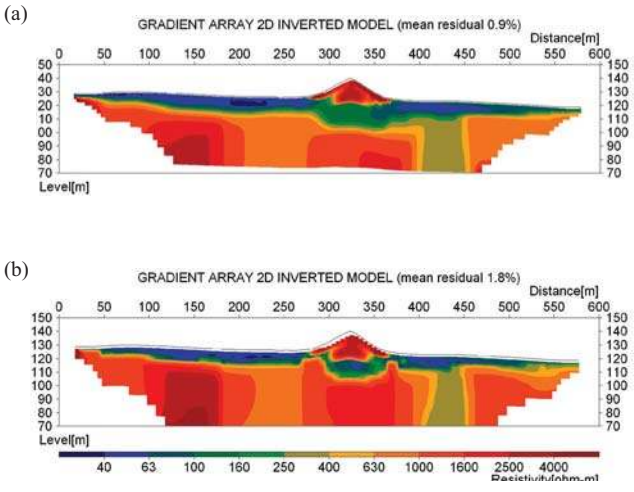

FIGURE 12

Inverted section from parallel line (approx. 60 m west) across the Knivsåsen esker, based on multiple-gradient array data: (a) 2.5 m model cells, (b) 5 m model cells.

material, with higher values to the south (>4000 Ωm) and not quite so high at the northern end of the section (1000–1600 Ωm). The high-resistivity bottom layer corresponds to the bedrock, and the change in resistivity at around 170 m may be interpreted as a fault. A low-resistivity zone centred around 365 m is evident; this is interpreted as a major fracture or fault zone. These interpretations are in accordance with the geological location of the survey over the edge of a major horst structure, where a number of subfaults and a variation in rock type can be anticipated. The corresponding inverted section based on Wenner data is shown in Fig. 11(b). The upper parts of the section are essentially similar to the gradient section with only minor differences. A very notable difference is, however, clearly visible in the bottom layer, where the low-resistivity zone is absent. The zone is clearly indicated in the corresponding dipole-dipole section (Fig. 11c), although the variation in depth to the bottom layer differs, and the resistivity of the bottom zone is markedly lower than for the other electrode arrays. Different inversion parameters were tested for the three electrode arrays, including lateral model grid sizes equal to the electrode spacing and to half the electrode spacing, but the presence of the low-resistivity vertical zone remains unchanged. The existence of the low-resistivity zone has also been shown in a gradient-array section measured parallel to the line, 60 m to the west (Fig. 12). For this profile, as well as the previously presented profile, the high-resistivity bottom layer appears to rise in narrow peaks below the edges of the esker (Fig. 12b) if the multiple-gradient array data are inverted with the coarser model grid division. These appear unrealistic from a geological point of view and are considered to be artefacts arising from difficulties experienced by the inversion routine in modelling the strong variation in the data with a coarser grid.

In a profile 40 m to the east of the line, the zone is weakly indicated in the inverted section based on dipole-dipole data, but is not visible for the other arrays or inversion parameters (not shown). This indicates that either the zone thins out or there is a fault between the lines. The fact that it is only indicated in the dipole-dipole data might be caused by higher sensitivity to 3D effects.

DISCUSSION

Results presented by Dahlin and Zhou (2004) clearly show that the gradient array with multiple current-electrode combinations is among the best electrode arrays in terms of resolution of subsurface structures for the five different numerical models tested, and it is clearly superior to the commonly used Wenner array in most of the modelled cases. Although it is not possible to evaluate the true resolution of the different electrode arrays due to lack of suitably detailed reference data from the test sites, the field experiments presented support these conclusions.

At the Härlöv site, the inverted sections from the Wenner and gradient array data agree well, but although the inverted dipole-dipole section is mostly similar, there are some features that differ. The general agreement between the inverted models from the Managua site is good for all three electrode arrays, although the Wenner model gives an impression of less detail. At the Knivsåsen site, inversion of both the dipole-dipole and multiple-gradient array data appears to have detected a fault zone that passed unnoticed with the Wenner array. The failure of the Wenner array to detect the fault may, to some extent, be an effect of reduced sensitivity towards the ends of the line, which can be expected to be more severe for the Wenner array, as judged by the sensitivity function. In general, however, the resolution of narrow structures at depth is expected to be lower for the Wenner array. The dipole-dipole array gave resistivities in the lower parts of the inverted models that deviated significantly from those obtained using the Wenner and gradient arrays, for both the Managua and Knivsåsen sites. One explanation might be that the sensitivity for the longest electrode layouts is focused towards the ends of the dipole-dipole electrode array (Fig. 2), giving a low relative sensitivity at depth in the lower central part of the model. This is particularly pronounced for the larger n-factors used for greater depth penetration, but a higher sensitivity to 3D structures from zones beside the survey line may also be part of the explanation. The inversion of gradient- array data, at least in some cases, as shown for the Knivsåsen site, requires that inversion is carried out with a grid division finer than one node between each electrode, in order to avoid artefacts.

In summary, the results demonstrate the applicability of the multiple-gradient array in real situations, and they support the advantages in terms of resolution capability and signal-to-noise ratio. A way of further optimizing the resolution capability may be to combine multiple gradient and dipole-dipole measurements. However, this is beyond the scope of this paper.

The formula suggested for pseudosection plotting is useful for data-quality checking, which is a valuable tool during data acquisition. However, in environments with significant lateral variation, plotting all the data for the multiple-gradient array in one pseudosection can give a false impression of noisy data. This is caused by close plotting of pseudosection points that are sensing different volumes of earth, i.e. they have significantly different distributions of the sensitivity function. This will occur for arrays where different combinations of *a*-spacings and *n*-factors are mixed in the same diagram, and similar effects would also occur if the pseudosection plotting points were based on integrating the sensitivity function to find its centre of gravity. Furthermore, for multiple-gradient-array data points using the same potential electrodes but mirrored current-electrode positions, the data points will be superimposed, so for a full visual assessment of the data quality it is worthwhile plotting the mirrored data sets separately. Hence, plotting one pseudosection for each *n*-factor, or *m*-factor, or alternatively one for each *a*-spacing, gives a better image for data-quality-assessment purposes.

The gradient array is highly suitable for multichannel data acquisition, which is not the case for some of the more commonly used electrode arrays such as the Wenner. From a practical point of view, the increased speed of measurement for multichannel gradient-array surveying compared to single-chan-

nel surveying is an immense practical advantage. When measuring in single-channel mode, the field crew will normally have to spend a significant part of a day in the field waiting for the instrument to carry out measurements, whereas for a multichannel gradient array, the pace of work of the field crew is the main limiting factor. In the former case, it is tempting to reduce the data density of the measurement protocols to speed up the data acquisition process, thus reducing the resolution capability of the Wenner array further (Dahlin and Loke 1998) and severely jeopardizing the quality of the survey. Occasional problems of this kind have been reported from, for example, Denmark, where the cost of field operations is high and competition between consultant companies is keen (pers. comm. from Dr. Esben Auken, The HydroGeophysics Group, Department of Earth Sciences, University of Aarhus, Finlandsgade 8, 8200 Århus N, Denmark). With the efficient measurement process of multichannel gradient-array surveying, the temptation to reduce the data density too far should be minimized. Stummer *et* al. (2004) concluded that an increase in data density to levels far above those that can be achieved with the Wenner array is beneficial for the resolution capability, which is a further motivation for using multichannel data acquisition. Another advantage of a high data density is that loss of data, due to, for example, skipped electrodes, is less serious as there is some redundancy in the data, and a larger number of noisy data points due to electrodes with poor grounding contact can be edited out, without compromising the quality of the inverted model significantly.

It is important to mention that induced-polarization (IP) measurements carried out along the Härlöv waste site test line clearly demonstrated that chargeability appears to be a key parameter for delineating buried waste (Leroux and Dahlin 2002). Thanks to the increased speed of multichannel gradient array, continued surveying at the site could economically be carried out measuring combined resistivity and IP, which would otherwise have been very time consuming and expensive.

If a data acquisition system with significantly more channels than is common today were available, or if longer electrode separations were employed, the gradient array would have a clear advantage over the dipole-dipole array in terms of signal-to-noise levels, as the latter would suffer if *n*-factors and electrode separations were increased. The results demonstrate the superiority of the multiple-gradient array, particularly for multichannel resistivity imaging, both in terms of improved resolution and measurement logistics, although the final choice of electrode array will also depend on the purpose of the investigation, site conditions and logistics.

CONCLUSIONS

The conclusions can be summarized as follows:

- The multiple-gradient array provides very stable field data acquisition, with good signal-to-noise ratio.
- It does not require a remote electrode, yet to some extent it has a sensitivity similar to the pole-dipole array.
- Inverted models based on multiple-gradient array data generally compare well with those based on Wenner and dipole-dipole data.
- The improved resolution of the multiple-gradient array compared to the Wenner array, found by previous numerical modelling, is supported by one of the field examples.
- A relatively fine grid division may be needed for the inversion in order to avoid artefacts.
- For data-quality assessment and editing purposes, apparent resistivities should preferably be plotted separately for different *n*-factors, or *m*-factors.
- The multiple-gradient array is well suited for multichannel data acquisition, but is also a good alternative for single-channel data acquisition.

ACKNOWLEDGEMENTS

The work for this paper was supported by a research grant from Civilingenjörsförbundets Miljöfond/Swedish Association of Graduate Engineers (Torleif Dahlin) and Wenner-Gren Foundation (Bing Zhou), which is gratefully acknowledged. The Härlöv field survey was part of a study financed by Kristianstads Kommun and carried out in cooperation with Tyréns Infrakonsult AB. The data acquisition was carried out by Virginie Leroux and Anna-Karin Jönsson. The field tests in Managua were carried out within a bilateral programme funded by Sida-SAREC, and could not have been done without the help of students and staff of CIGEO at UNAN-Managua.

REFERENCES

Bernstone C., Dahlin T., Ohlsson T. and Hogland W. 2000. DC resistivity mapping of internal landfill structures: Two pre-excavation surveys. *Environmental Geology* **39**, 360–371.

Dahlin T. 1996. 2D resistivity surveying for environmental and engineering applications. *First Break* **14**, 275–283.

Dahlin T. and Loke M.H. 1997. Quasi-3D resistivity imaging: mapping of 3D structures using two dimensional DC resistivity techniques. Proceedings of the 3rd Environmental and Engineering Geophysics Meeting, Aarhus, Denmark, pp.143–146.

Dahlin T. and Loke M.H. 1998. Resolution of 2D Wenner *resistivity* imaging as assessed by numerical modelling. *Journal of Applied Geophysics* **38**, 237–249.

Dahlin T. and Zhou B. 2004. A numerical comparison of 2D resistivity imaging with ten electrode arrays. *Geophysical Prospecting* **52**, 379–398.

Edwards L.S. 1977. A modified pseudosection for resistivity and induced-polarization. *Geophysics* **42**, 1020–1036.

Ekström G. 1961. *Beskrivning till kartbladet Revinge*. Serie Ad, Nr 3, Sveriges Geologiska Undersökning (Swedish Geological Survey), Stockholm.

Hradeck_ P., Havlicek P., Hradeck_ P., Navarro M., Novak Stanik Z.E. and Sebesta J. 1997. *Estudio Geológíco para reconocimiento de riesgo natural y vulnerabilidad geológia en el área de Managua*. Report, _esk_ Geologick_ Ústav – INETER (Instituto Nicaragüense de Estudios Territoriales), Prague-Managua.

Leroux V. and Dahlin T. 2002. Induced polarisation survey at a waste site in southern Sweden. Proceedings of the 8th Environmental and Engineering Geophysics Meeting, Aveiro, Portugal, pp. 207–210.

Loke M.H., Acworth I. and Dahlin T. 2003. A comparison of smooth and blocky inversion methods in 2-D electrical imaging surveys. *Exploration Geophysics* **34**, 182–187.

Loke M.H. and Barker R.D. 1995. Least-squares deconvolution of apparent resistivity pseudosections. *Geophysics* **60**, 1682–1690.

McGillivray P.R. and Oldenburg D.W. 1990. Methods for calcu lating Frechet derivatives and sensitivities for the non-linear inverse problem: A comparative study. Geophysical *Prospecting* **38**, 499–524.

Parrales R., Dahlin T. and Rubí C. 2003. Site investigation with combined methods in a faulted area in Managua, Nicaragua - a pre-study. Proceedings of the 9th European Environmental and Engineering Geophysics Meeting, Prague, Czech Republic, pp.

Ringberg B. 1980. *Beskrivning till jordartskartan Malmö SO*. Serie AE, Nr 38, Sveriges Geologiska Undersökning (Swedish Geological Survey), Uppsala.

Stummer P., Maurer H. and Green A. 2004. Experimental design: Electrical resistivity data sets that provide optimum subsurface information. *Geophysics* **69**, 120–139.

Zhou B. and Dahlin T. 2003. Properties and effects of measurement errors on 2D resistivity imaging surveying. *Near Surface Geophysics* **1**, 105–117.